Miranda cargo-binding domain forms an elongated coiled-coil homodimer in solution: Implications for asymmetric cell division in *Drosophila*

MOHAMMAD S. YOUSEF,[1,2,3] HIRONARI KAMIKUBO,[4] MIKIO KATAOKA,[4] RYUICHI KATO,[1] AND SOICHI WAKATSUKI[1]

[1]Structural Biology Research Center, Photon Factory, IMSS, High Energy Accelerator Research Organization, Tsukuba, Ibaraki 305-0801, Japan
[2]Biophysics Department, Faculty of Science, Cairo University, Giza, Egypt
[3]Center for Advanced Interdisciplinary Sciences (CAIS), Biotechnology Division, Faculty of Science, Cairo University, Giza, Egypt
[4]Graduate School of Materials Science, Nara Institute of Science and Technology, Ikoma, Nara 630-0192, Japan

(RECEIVED January 2, 2008; FINAL REVISION February 15, 2008; ACCEPTED February 15, 2008)

Abstract

Miranda is a multidomain adaptor protein involved in neuroblast asymmetric division in *Drosophila melanogaster*. The central domain of Miranda is necessary for cargo binding of the neural transcription factor Prospero, the Prospero-mRNA carrier Staufen, and the tumor suppressor Brat. Here, we report the first solution structure of Miranda central ''cargo-binding'' domain (residues 460–660) using small-angle X-ray scattering. Ab initio modeling of the scattering data yields an elongated ''rod-like'' molecule with a maximum linear dimension (D_{max}) of ~22 nm. Moreover, circular dichroism and cross-linking experiments indicate that the cargo-binding domain is predominantly helical and forms a parallel coiled-coil homodimer in solution. Based on the results, we modeled the full-length Miranda protein as a double-headed, double-tailed homodimer with a long central coiled-coil region. We discuss the cargo-binding capacity of the central domain and propose a structure-based mechanism for cargo release and timely degradation of Miranda in developing neuroblasts.

Keywords: Miranda; *Drosophila*; asymmetric cell division; coiled coil; SAXS

Supplemental material: see www.proteinscience.org

During embryonic development of the *Drosophila* central nervous system, mitotic neuroblasts divide asymmetrically to produce different daughter cells: another neuroblast (self-renewal), and a smaller ganglion mother cell (GMC) that is destined to differentiate. Each GMC typically divides once more into a pair of fully developed neurons (Betschinger and Knoblich 2004; Yu et al. 2006). In this regard, the term ''asymmetric division'' refers to pre-programmed differences in daughter cells' morphology, gene expression, developmental potential, and fate. The asymmetric cell division effectively leads to cell type diversity by making two kinds of cells out of one. The main cause of the asymmetry is that several protein determinants are unequally distributed within the mitotic neuroblast prior to or during cytokinesis. Subsequently, these determinants are unequally partitioned among daughter cells, leading to different cell fates (Wodarz and Hutter 2003; Wodarz 2005). The underlying molecular mechanism of the asymmetric distribution of cell fate determinants within developing cells remains a fundamental question in cell and developmental biology.

Reprint requests to: Mohammad S. Yousef, Structural Biology Research Center, Photon Factory, IMSS, High Energy Accelerator Research Organization, Tsukuba, Ibaraki 305-0801, Japan; e-mail: yousef@post.kek.jp; fax: 81-29-879-6179.

Article published online ahead of print. Article and publication date are at http://www.proteinscience.org/cgi/doi/10.1110/ps.083431408.

Miranda, a multidomain protein (830 residues), is preferentially segregated to the GMC upon cell division. An essential cell fate determinant, the transcription factor protein Prospero binds to the central domain of Miranda and subsequently segregates with Miranda to the GMC (Shen et al. 1997). Prospero specifies the GMC fate by repressing neuroblast genes and activating GMC genes, which then direct the cells toward differentiation (Choksi et al. 2006). As a backup mechanism, the Prospero-mRNA carrier protein Staufen also interacts with the central domain of Miranda and asymmetrically segregates into the GMC (Shen et al. 1998). Additionally, another cell fate determinant protein, Brat, was recently shown to bind the central domain of Miranda and co-localizes with Prospero and Staufen. Brat not only controls GMC proliferation, but also somehow facilitates the complete segregation of Prospero (Betschinger et al. 2006; Lee et al. 2006).

Thus, Miranda, through its central domain, coordinates the asymmetric segregation of the cargos Prospero, Staufen, and Brat into the GMC. Once in the GMC, Miranda is rapidly degraded, and the cargos are released (Schuldt et al. 1998).

Miranda associates with the apical cortex of dividing neuroblasts during interphase and then localizes to the basal cortex in metaphase (Peng et al. 2000). It is not clear exactly how Miranda translocates between the two poles during the cell cycle. It is known, however, that the N terminus of Miranda (residues 1–290) is sufficient for its membrane association, whereas the C terminus (residues 727–830) is required for its efficient cortical localization (Slack et al. 2007), timely degradation, and cargo release (Fuerstenberg et al. 1998). The central domain of Miranda is predicted to form one or more long coiled coils on which binding sites for Prospero, Staufen, and Brat seem to overlap (Schuldt et al. 1998; Shen et al. 1998; Lee et al. 2006). Each of the overlapping cargo-binding sites is significantly long, consisting of more than 100 residues. It is not known whether a single molecule of Miranda could carry multiple cargos simultaneously and whether the cargos bind independently, cooperatively, or competitively. The lack of sequence homologies and structural information of Miranda protein hinders sufficient elucidation of its cargo-binding and release mechanisms.

In this report, we characterized a truncated segment of the central domain of Miranda (residues 460–660) and obtained its first solution structure. The region contains binding sites for the cargos Prospero, Staufen, and Brat; thus, it is named the cargo-binding domain (CBD). The results showed that Miranda CBD forms an elongated ''rod-like,'' parallel coiled-coil homodimer. Moreover, the results help us speculate the cargo-binding capacity of the Miranda central domain, build a model for the entire protein, and propose a cargo release mechanism.

Results

Miranda CBD is predominantly helical and mostly coiled coil

Based on primary sequence analysis, Miranda CBD is predicted to be predominantly helical with a high propensity for coiled-coil formation (Fig. 1A,B). Coiled coils are autonomous folding units consisting of at least two α-helices that wrap around each other with a slight left-handed superhelical twist (Cohen and Parry 1990). Coiled-coil sequences are characterized by a heptad repeat pattern of seven residues, denoted $(a,b,c,d,e,f,g)_n$, in which residues in positions a and d are mostly hydrophobic while the remaining positions (b, c, e, f, g) are generally charged or polar. The stability of the coiled coil is derived mainly from a characteristic packing of the hydrophobic side chains (in positions a and d) into a hydrophobic core (''knobs into holes'') (Crick 1953). Additionally, charged residues, especially those in positions g and e (Zhou et al. 1994a,b), can form intra- and interhelical interactions and thus may contribute to the coiled-coil stability and chain registry (Kohn et al. 1995, 1997, 1998). By computational methods, such patterns of hydrophobic and polar residues can be used to predict coiled-coil domains in amino acid sequences (Lupas et al. 1991; McDonnell et al. 2006).

Using the program COILS (see Materials and Methods), we identified a continuous stretch of 18 heptad repeats, spanning from residues 484 to 609. The long coiled coil is flanked by shorter segments of non-coiled coil, yet helical, regions (Fig. 1A,B). When the helical wheel projection of the predicted heptad repeats was drawn, assuming a parallel coiled-coil homodimer, we could identify putative core and surface regions of the CBD (Fig. 1C).

The CD spectrum of Miranda CBD (Fig. 2A) is consistent with the predicted high helical content and also with a high degree of coiling. The CD spectrum with equal double minima of molar ellipticity at 208 and 222 nm is characteristic of coiled-coil structures. Because the n–π^* transition (222 nm) is mainly indicative of the α-helical content, whereas the π–π^* transition (208 nm) polarizes parallel to the helix axis, the ellipticity ratio $[\theta]_{222}/[\theta]_{208}$ is often used as an indicator for the occurrence of stable α-helical coiled coils. The value of this ratio is 1.04 for Miranda CBD (Fig. 2A), consistent with a stable coiled-coil formation (Lau et al. 1984; Cooper and Woody 1990; Zhou et al. 1992). The helical content of Miranda CBD, based on the $[\theta]_{222}$ value, was calculated to be about 75%–80% (see Materials and Methods).

Miranda CBD is homodimeric

Coiled-coil proteins are usually dimers, but they also can arrange in higher oligomeric states (trimers, tetramers, and pentamers) (Mason and Arndt 2004). To investigate

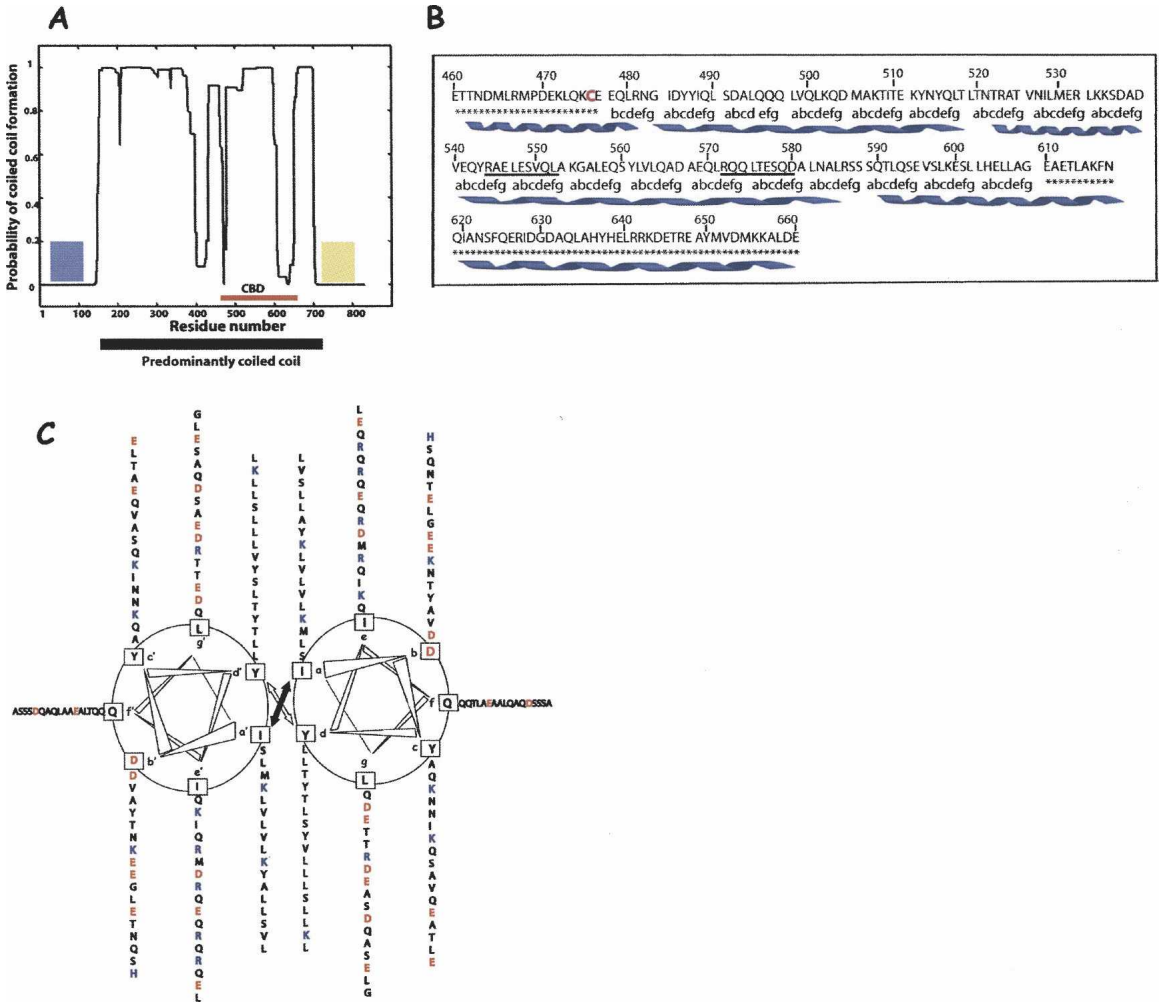

Figure 1. Sequence analysis of Miranda CBD. (*A*) Probability of coiled-coil formation of the full-length Miranda protein predicted by the program COILS (Lupas et al. 1991). The cyan and yellow boxes represent the extreme N and C termini (non-coiled coil), respectively. The position of Miranda CBD (residues 460–660) is indicated by the red bar. (*B*) Amino acid sequence of the Miranda CBD. The predicted helical regions are indicated as blue ribbons. The predicted heptad repeats are denoted as ''abcdefg'' and the asterisks (*) indicate non-coiled-coil regions. Two potential destruction boxes are underlined. A single N-terminal cysteine (C476) is highlighted in pink. (*C*) Helical wheel representation of a dimeric coiled coil based on the predicted heptad repeats (residues 484–609). The view is from the N to the C terminus. Arrows depict the interactions in the hydrophobic core. Positively and negatively charged residues are colored in blue and red, respectively.

the oligomeric state of Miranda CBD, we first used MALDI-TOF (matrix-assisted laser desorption ionization time-of-flight) mass spectroscopy. Mass spectroscopy generally reveals the molecular masses of possible oligomeric states of dehydrated protein samples (Kulkarni and Rao 2006). The mass spectrum of Miranda CBD showed two sharp peaks unequivocally corresponding to masses of both the monomeric and dimeric forms (Fig. 2B). To further assess the oligomerization state, we carried out a chemical cross-linking experiment using a lysine-specific cross-linker (Fig. 2D). In addition to the monomer band that was observed exclusively in the absence of the cross-linker, a new band appeared with increasing concentrations of the cross-linker. The new band migrates at ~47 kDa corresponding to the dimeric form of Miranda CBD. No bands corresponding to higher oligomeric states were observed.

Miranda CBD forms parallel coiled coil

The α-helical chains in a coiled coil can align in either parallel or antiparallel orientation (Monra et al. 1993), i.e., aligned with the peptide backbones pointing in the same (parallel) or in the opposite (antiparallel) directions. In order to determine the orientation of the interacting helices, we used a single N-terminal cysteine (C476, highlighted in pink, Fig. 1B) as a probe. The probe

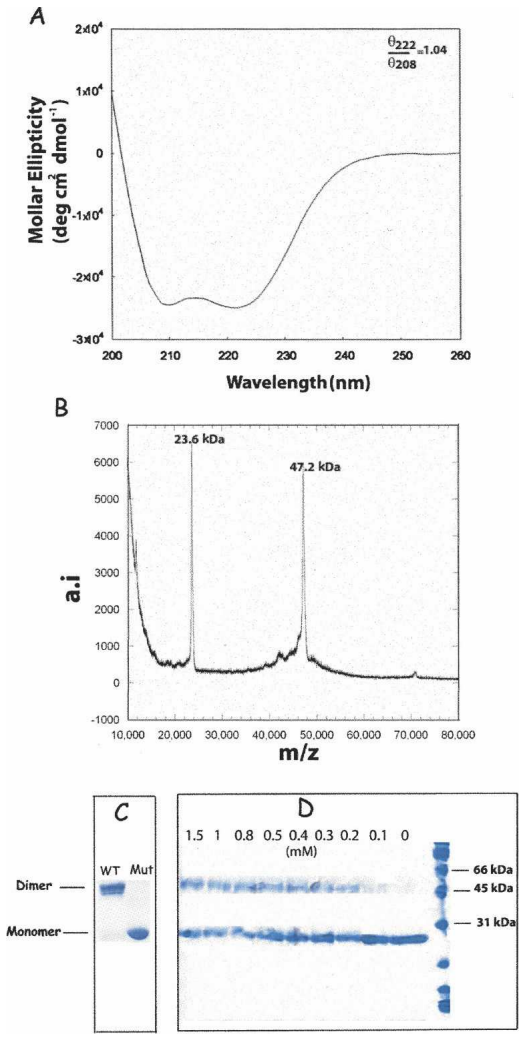

Figure 2. Biophysical and biochemical characterizations of Miranda CBD. (*A*) The CD spectrum at 20°C is indicative of a predominantly helical structure with a high degree of coiling. (*B*) MALDI-TOF mass spectrum of a dehydrated sample shows two sharp peaks that correspond to the monomeric and dimeric states of Miranda CBD. (*C*) Nonreducing SDS-PAGE of the wild-type (WT, *left* lane) and C476S mutant protein (Mut, *right* lane). The dimer band indicates a disulfide bridge formation between the corresponding N-terminal cysteines (C476) in the wild-type but not in the mutant protein. (*D*) Chemical cross-linking of Miranda CBD using increasing concentrations (in mM) of the lysine cross-linker EGS (see Materials and Methods). Cross-linked products are separated on reducing SDS-PAGE. A dimer band emerges as the concentration of the cross-linker increases. The molecular weight marker lane serves for the gel pattern in *C*, as well.

cysteine is not part of the predicted heptad repeats. Therefore, only when the interacting helical chains align in register and in a parallel orientation can a disulfide bridge form between the corresponding cysteines. To explore the formation of a disulfide bridge, we tested a wild-type protein sample (DTT-free) by nonreducing SDS-PAGE. On the gel, a strong single band that corresponds to the dimeric form appeared (Fig. 2C). When the "probe" cysteine is mutated to serine (C476S mutant), again only a single band appeared, but this time corresponding to the monomeric form. The result indicates that the two helical chains of Miranda CBD are covalently linked via a disulfide bridge in nonreducing conditions, suggesting a parallel coiled-coil orientation.

Miranda CBD is elongated

We used the small-angle X-ray scattering method (SAXS) to characterize the molecular shape of Miranda CBD in solution (Fig. 3). The values of the radius of gyration *Rg* and forward scattering *I*(0) were determined by Guinier approximation (see Materials and Methods). The concentration dependences of R_g^2 and *I*(0)/conc are shown in Figure 3, B and C, respectively. These parameters remain constant within the errors, and the intrinsic values of *I*(0)/conc and R_g were estimated to be 7100 (±300) and 5.3 (±0.1) nm by averaging the data. Compared with the value of *I*(0)/conc of ovalbumin (43 kDa), 7700 (±150), the apparent molecular weight of Miranda CBD was evaluated to be ~40 kDa, which is somewhat smaller than that expected for a dimer (47.2 kDa).

Next, the pair-distance distribution function *P*(r) of Miranda CBD (Fig. 3D) was calculated using a maximum particle dimension (D_{max}) of 21.7 nm (determined from the shape analysis mentioned below). The peak position is located at r ~2 nm, and the profile exhibits a linear decrease with the increase of r in the higher r region, which is a characteristic feature of an elongated rod-like particle (Glatter and Kratky 1982). Using the value of *I*(0)/conc obtained from the *P*(r) analysis, the apparent molecular weight was estimated to be 45 kDa, which is very close to that of the dimeric CBD (47.2 kDa). The *P*(r) function gave an *I*(0)/conc of 8100 (±500) and R_g of 6.5 (±0.5) nm, respectively. Comparing the values of R_g and *I*(0)/conc from Guinier analysis with those obtained from the *P*(r) function, the former are slightly smaller than the latter. It must be kept in mind, however, that in the case of a significantly elongated rod-like particle, the Guinier approximation can be applied only to a relatively small angle region compared with that of spherical particles. Therefore, for Miranda CBD, there is good reason to suspect that the present fitting region ($Q^2 < 0.07$ nm^{-1}) in the Guinier analysis is far from ideal, and, subsequently, the obtained Guinier parameters may not be accurate. On the other hand, the analysis of the *P*(r) function (calculated using the overall scattering profile) is tolerant to the limitation of the small angle resolution, resulting in significantly more reliable estimates of molecular weight and R_g values.

The gross structure of Miranda CBD was restored ab initio from the scattering pattern using the shape determination program GASBOR (see Materials and Methods). All independent reconstructions yielded reproducible shapes

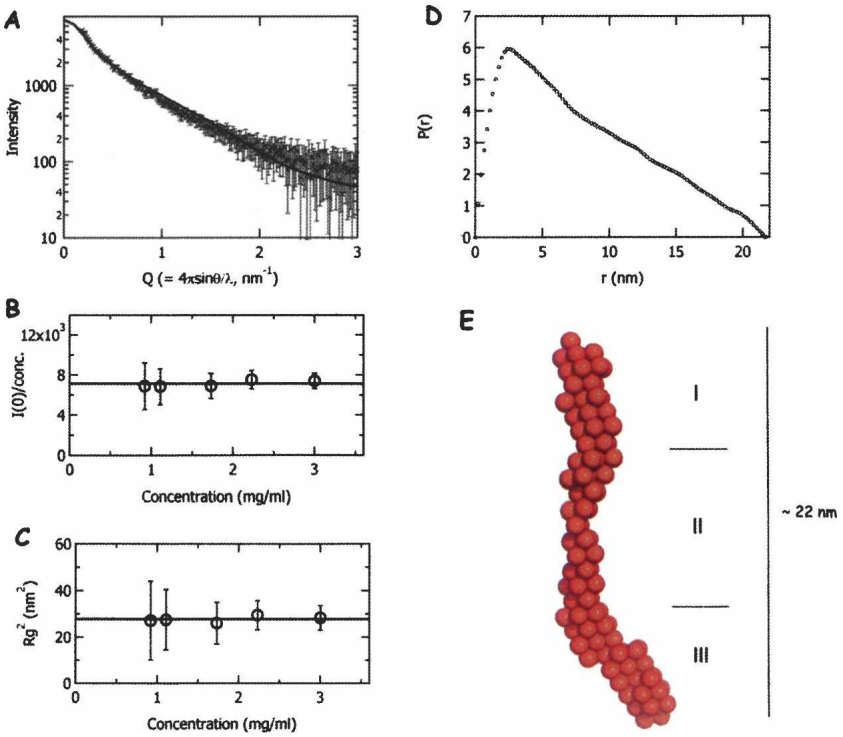

Figure 3. Small angle X-ray scattering (SAXS) analysis of Miranda CBD. (*A*) The averaged small-angle X-ray scattering profile of Miranda CBD. The solid continuous curve shows the calculated scattering profile of the obtained model structure. (*B*) The concentration dependence of R_g^2 and (*C*) *I*(0)/conc., obtained from the Guinier analysis. The solid line in each panel represents the average value of the five data points. (*D*) The *P*(r) function of Miranda CBD, computed from the SAXS data using the program GNOM (see Materials and Methods). (*E*) Low-resolution, ab initio, SAXS model of Miranda CBD consists of three distinct regions (see text). Dummy residues (red) are shown in space-filling mode.

with similar structural features and have been averaged. The averaged maximum dimension of Miranda CBD was found to be 21.7 (±0.2) nm. The convergent feature of the reconstructed models suggests that Miranda CBD adopts a definitive molecular shape in solution within the experimental resolution. Moreover, the averaged shape produced a good fit to the experimental data ($\chi^2 = 0.99$) in the entire scattering range (Fig. 3A). Miranda CBD appeared as an elongated rod-like molecule consisting of three distinct regions, I, II, and III, and with kinks at both ends (Fig. 3D). The average widths of regions I, II, and III were ~1.3, 1.0, and 1.8 nm, respectively.

Dynamic Light Scattering (DLS) measurements provided additional evidence of the monodispersity and elongated structure of the molecule (see Supplemental information). The hydrodynamic radius of Miranda CBD was estimated to be ~7.5 nm.

Discussion

Structural features of Miranda CBD

SAXS experiments along with biochemical and biophysical characterizations showed that Miranda CBD forms a parallel coiled-coil homodimer in solution and adopts an elongated (~22 nm) rod-like structure. In the SAXS model (Fig. 3E), Miranda CBD somewhat resembles an extended rope with terminal kinks. The average width of the middle region II of Miranda CBD is relatively smaller than those at terminal regions I and III (1.0, 1.3, and 1.8 nm, respectively). The change in the width at both ends of the model could be ascribed to unwinding of the coiled coil at these regions. That is consistent with the coiled-coil propensities predicted for the CBD (Fig. 1A), where non-coiled-coil regions exist at both ends. Assuming that the width of the molecule reflects the interhelical distance of the coiled coil, the middle region II appears to correspond to the long stretch of heptad repeats (shown in Fig. 1C) with strong interhelical interactions. The width of region II (1.0 nm) is indeed very close to the interhelical distance of canonical coiled coils (~0.96 nm) (O'Shea et al. 1991).

The parallel orientation of the coiled-coil homodimer is biologically meaningful. As noted before, the N terminus of Miranda protein (residues 1–290) associates with the cell cortex. Therefore, the N termini of two interacting molecules would, conceivably, point toward the same direction in the cell. To bring two interacting monomers

together via self-association of the central domains, the parallel conformation seems plausible. Moreover, from the predicted helical wheel of the Miranda CBD coiled-coil region (Fig. 1C), the parallel arrangement of a homodimer seems favorable. The charged residues in positions g/g′ are mostly of negative signs while those in positions e/e′ are more basic, potentially destabilizing the antiparallel form (through repulsive g–g′ and e–e′ interactions). That is consistent with the result of the cysteine cross-linking experiment (Fig. 2C), which strongly suggests the formation of a parallel dimer.

Cargo binding capacity of Miranda CBD

It is not unusual for long homodimeric coiled coils to bind multiple protein partners simultaneously, on nearby sites, without steric clashes. This is primarily due to the extended nature of the coiled coil and the formation of two opposing interfaces available for interaction. One extreme example is the long coiled coil of the tropomyocin protein, which has numerous binding sites for actin and at the same time binds distinct regions of troponin (Brown et al. 2005). There are also cases in membrane trafficking where long homodimeric coiled-coil proteins help assemble multiple protein partners required for membrane fusion. A representative example is the C-terminal coiled-coil region of the FIP3 protein, which is involved in membrane trafficking from recycling endosomes to the plasma membrane during cytokinesis. The crystal structure of the Rab11 protein in complex with FIP3 revealed the capacity of the FIP3 parallel coiled-coil homodimer to bind two copies of the Rab11 protein on its symmetrical opposing interfaces (Eathiraj et al. 2006; Shiba et al. 2006). A longer stretch of FIP3 (150 residues, mostly in coiled coil) was shown to bind not only two copies of Rab11 but also the ARF5 protein simultaneously (Shiba et al. 2006; Horgan et al. 2007).

Moreover, on coiled-coil regions, even when the binding to a protein partner is mediated by several adjacent amino acids, a much longer stretch of the coiled coil may be required to stabilize the binding. One example is the interaction between the catalytic GEF coiled-coil homodimer of Sec2p in complex with its Rab partner Sec4p. A minimum parallel coiled-coil length of about 130 residues was required for the efficient binding and catalysis of nucleotide exchange (Sato et al. 2007b). However, only about a dozen adjacent residues of the coiled coil were shown to directly contact the protein partner in the complex crystals (Dong et al. 2007; Sato et al. 2007a). This was ascribable to the lack of stability of the shorter coiled coils, and longer stretches of coiled coils help provide sufficient ''rigidity'' to the ''confined'' binding sites. In this regard, segments on Miranda CBD identified as minimum binding sites for the cargo proteins Prospero (residues 468–648) (Shen et al. 1998), Staufen (residues 506–638) (Schuldt et al. 1998), and Brat (residues 481–579) (Lee et al. 2006) are expected to be much longer than the actual regions of contact, which, in turn, could be distinct for each cargo. In other words, the apparent overlap of the binding sites could be merely due to a structural requirement for stable coiled-coil formation. This is consistent with the recent evidence that one of the cargo proteins, Brat, is required for the proper segregation of another cargo, Prospero, during the asymmetric cell division of developing neuroblasts. One explanation is that Brat stabilizes Prospero binding on Miranda CBD, which in turn suggests a possible cooperative binding of the two cargos on nearby sites (Lee et al. 2006).

At this stage, we speculate that the dimeric Miranda CBD is structurally capable of binding multiple cargos simultaneously on its elongated coiled-coil region and the unwound termini. Obviously, final confirmation awaits further structural and biochemical analyses of Miranda CBD bound to its cargos.

Proposed structure–function relationship

Based on the primary sequence analysis, Miranda full-length protein is predicted to contain a long central domain of coiled coils (residues 150–700) flanked by non-coiled-coil N and C termini (Fig. 1A). Here, we have shown that Miranda CBD (residues 460–660) dimerizes into an elongated parallel coiled-coil structure. Because the CBD is part of the long central domain, the same structural trend, i.e., the shape, orientation, and oligomerization, is likely to continue throughout the central coiled-coil region of Miranda. Therefore, the central domain of Miranda is expected to serve as a dimerization motif for the entire protein via parallel coiled-coil self-association. We suggest a model for the entire protein, simplified in Figure 4, in which Miranda forms a double-headed and double-tailed homodimer with a long central coiled-coil region.

Miranda is not detectable in cells after cytokinesis, suggesting that Miranda degradation is a prerequisite for the release of the cargos. Miranda contains four potential destruction boxes, a 9 amino acid motif originally identified in A and B cyclins, that are involved in their cell-cycle-dependent degradation (King et al. 1996; Shen et al. 1997). Two of these destruction boxes are located within the CBD coiled-coil region (residues 544–552 and 572–580), whereas the other two lie N-terminal to the CBD (residues 356–364 and 431–439) (Figs. 1B, 4). The coiled-coil structure of the CBD, along with the cargo binding, is expected to shield the destruction boxes, rendering them inaccessible to potential degradation pathways.

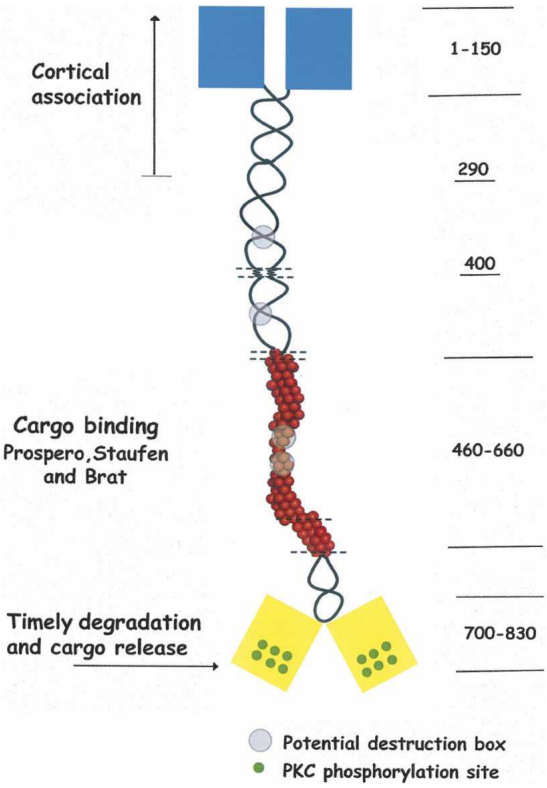

Figure 4. Model of the overall structure of Miranda protein. A cartoon representation of full-length Miranda based on the ab initio SAXS model of the CBD (balls in red). Residue numbers are shown on the *right*. Green circles at the C-terminal region represent phosphorylation sites. Gray circles indicate four potential destruction boxes (see text). Predicted non-coiled-coil regions are indicated by dotted lines. Cyan and yellow boxes (as in Fig. 1) represent the N and C termini, respectively.

On the other hand, the extreme C-terminal 103 amino acids (residues 727–830) were found to be essential for cargo release and the timely degradation of Miranda. The C-terminal region of Miranda contains multiple consensus protein kinase C phosphorylation sites, raising the possibility of phosphorylation-dependent degradation (Ikeshima-Katoka et al. 1997). Based on our model of full-length Miranda (Fig. 4), phosphorylation at the C termini could lead to unfavorable electrostatic interactions between and/or structural changes of the identical double-tails of the Miranda dimer. These changes could destabilize (unzip) the nearby coiled coil and the CBD. When unzipped, the CBD would not only release the bound cargos but also expose the destruction boxes. That is consistent with the observation that replacing the extreme C terminus of Miranda, which contains the consensus phosphorylation sites, with a segment of unrelated (non-phosphorylatable) residues prevents cargo release (Ikeshima-Katoka et al. 1997). The proposed mechanism implies that the degradation of Miranda is a consequence rather than the cause of cargo release.

Additionally, the first 290 residues of Miranda protein are known to be sufficient for its membrane association. About half of the residues (residues 150–290) can form coiled coil (Fig. 1A). Although it is not known exactly which molecule(s) tether Miranda to the cell cortex, the dimerization of the two identical N-terminal domains forming the double-heads of the Miranda dimer (Fig. 4) might be required to increase avidity for specific binding partners.

In summary, our data suggest that the central coiled-coil domain of Miranda protein forms an extended dimerization motif for the entire protein. We propose that the stability and cargo-binding capacity of the central domain could be regulated by phosphorylation at the C terminus.

Materials and Methods

Bioinformatics

Coiled-coil propensities were estimated using the program COILS (http://www.ch.embnet.org/software/COILS_form.html) (Lupas et al. 1991) using a window width of 28. Similar results were obtained using the program Paircoil2 (data not shown), (http://groups.csail.mit.edu/cb/paircoil2/paircoil2.html) (McDonnell et al. 2006). Secondary structure prediction was performed using the consensus sequence option implemented in the network of protein sequence analysis (http://npsa-pbil.ibcp.fr) (Combet et al. 2000).

Cloning of Miranda CBD

The DNA fragment encoding Miranda CBD domain (residues 460–660) was amplified by PCR using *Miranda* cDNA (NCBI, id: AB005661) as a template and a pair of primers specific to the CBD domain.

Forward primer 5′-GAGACCACCAATGATATGCTG-3′
Reverse primer 5′-TTATTCATCGAGCGCCTTCTTCATGTCC-3′

BamHI and EcoRI cleavage sites were included at the ends of the forward and the reverse primers, respectively. After PCR, the amplified DNA product was purified from the mixture using the QIAquick PCR purification kit (Qiagen) and digested by the two restriction enzymes simultaneously. The digested DNA was then recovered from a 1% agarose gel using the QIAquick gel extraction kit (Qiagen) and cloned into the GST fusion expression vector pGEX 6P-1 (GE Healthcare). The nucleotide sequence of Miranda CBD was confirmed by DNA sequencing.

Expression and purification of Miranda CBD

GST-fused protein was expressed in *Escherichia coli* strain BL21(DE3) when induced with 0.25 mM isopropyl-β-D-thiogalactoside (IPTG), for 12 h at 25°C. Bacterial pellets were harvested by centrifugation at 10,000*g* for 10 min at 4°C. The

cells were then resuspended in PBS buffer (containing 500 mM NaCl, 10% glycerol, pH 7.0) and lysed by sonication on ice. The supernatant, recovered by centrifugation at 15,000*g* for 30 min, was loaded on a Glutathione-Sepharose 4B (GE Healthcare) column and incubated overnight at 4°C. The soluble fused protein was then eluted with glutathione and cleaved with PreScission protease (GE Healthcare). To remove the cleaved GST protein, the digestion mixture was dialyzed against low-salt (10 mM NaCl) buffer and loaded on anion exchange mono-Q column (GE Healthcare). Miranda CBD was eluted with an increasing salt gradient (10–800 mM NaCl). Miranda CBD was further purified by a Superdex 75 (Hiload 26/60, GE Healthcare) column (in buffer, 50 mM Tris·HCl, pH 7.5, 150 mM NaCl, 1 mM DTT, 10% glycerol). Out of a 4-L LB culture, 5–6 mg of purified protein was recovered. The final purity of the protein was tested by SDS-polyacrylamide gel electrophoresis (SDS-PAGE) (Laemmli 1970).

CD spectroscopy

CD spectrum of Miranda CBD (0.02 mM) in buffer (50 mM Tris-HCl, pH 7.5, 150 mM NaCl, 1 mM DTT, 5% glycerol) was recorded at 20°C by using a 0.1-cm cell on a Jasco J-810 spectropolarimeter. The spectrum was presented as an average of five scans recorded from 260 nm to 200 nm at a rate of 50 nm/min. The resulting data were baseline-corrected by buffer subtraction. The recorded spectrum in millidegrees of ellipticity (θ) was converted to mean residue ellipticity $[\theta]$ in deg cm^2 dmol^{-1} (Myers et al. 1997). The helical content was calculated, based on the value of $[\theta]_{222}$, using the equations described in Chen et al. (1972) and Richardson and Makhatadze (2004), and also using the program K2D (http://www.embl-heidelberg.de/~andrade/k2d/) (Andrade et al. 1993).

Mass spectroscopy

A purified protein sample (3 mg/mL) of Miranda CBD was analyzed using MALDI-TOF mass spectroscopy. The sample was mixed (1:5) with saturated matrix solution, consisting of sinnapinic acid, and dried on a stainless steel plate prior to the analysis. Mass spectrometry was performed using a Bruker autoflex-M2 MALDI-TOF mass spectrometer operating in the linear mode with internal calibration. Masses of possible oligomeric states were calculated using Bruker software.

Chemical cross-linking

Miranda CBD (1 mg/mL) in 50 mM HEPES, pH 7.5, 150 mM NaCl, 10% glycerol, 1 mM DTT was cross-linked with ethyleneglycol bis(-succinimidylsuccinate) (EGS, Fluka). The reaction mixtures were incubated for 1 h on ice at concentrations of 0, 0.1, 0.2, 0.3, 0.4, 0.5, 0.8, 1, and 1.5 mM EGS and then quenched with 50 mM glycine. Cross-linked products were analyzed under reducing conditions by SDS-PAGE (15% polyacrylamide).

Site-specific mutagenesis (C476S mutation)

A single cysteine (C476) at the N terminus of the construct was mutated to serine by Pfu-based PCR using the QuikChange site-directed mutation kit protocol (Stratagene) and the following primer pair:

5′-GACGAGAAGCTGCAGAAAAGCGAAGAGCAATTGCGC-3′
5′-GCGCAATTGCTCTTCGCTTTTCTGCAGCTTCTCGTC-3′

The cysteine to serine mutation was confirmed by DNA sequencing. The mutant protein was expressed and purified by the same procedure used for the wild type with the exception that DTT was not added during purification. The purified mutant protein was analyzed and compared with the wild type (DTT-free) under nonreducing conditions on SDS-PAGE (15% polyacrylamide).

Small-angle X-ray scattering

SAXS measurements were carried out at BL-10C, Photon Factory, Tsukuba, Japan (Ueki et al. 1985). The wavelength of X-rays was 1.488 Å as selected by a pair of Si (111) monochrometer crystals. The scattering profiles were collected using a position-sensitive proportional detector, PSPC, (RIGAKU). Samples of Miranda CBD were diluted in a buffer containing 50 mM Tris-HCl (pH 7.5), 250 mM NaCl, 10% glycerol, and 1 mM DTT. The scattering profiles of five successive protein concentrations (0.92, 1.11, 1.73, 2.23, and 3.0 mg/mL) were collected at 20°C (sample cell was of 1-mm path length). The exposure time was 5 min for each concentration. To improve the signal-to-noise ratio, five sets of independent measurements were averaged after checking each data for radiation damage.

In a small-angle region ($QR_g < 1.3$ for a spherical particle), a scattering intensity profile, $I(Q)$, can be approximated with the following equation (Guinier approximation) (Guinier and Fournet 1955):

$$I(Q) = I(0)\exp[-R_g^2(Q^2/3)], Q = 4\pi \sin\theta/\lambda,$$

where $I(0)$ is scattering intensity at $\theta = 0$ and R_g is a radius of gyration. The slope and the Y-intersection of a $\ln(I[Q])$ vs. Q^2 plot, Guinier plot, give $-R_g^2/3$ and $\ln I(0)$, respectively. The concentration-normalized intensity at zero angle, $I(0)$/conc., is generally proportional to the molecular weight of the sample. Scattering profiles from ovalbumin from chicken egg (43 kDa, Sigma A2512) dissolved in the same buffer were measured as a standard solution. The apparent molecular weight of Miranda CBD was estimated by comparison with the concentration-normalized forward scattering of ovalbumin solution. The pair distance distribution function, $P(r)$, was calculated using the program GNOM (Svergun 1992). Due to the short Guinier region of rod-like particles, D_{max} could not be calculated directly from the program GNOM and instead, was obtained from the shape prediction analysis (mentioned below). The apparent molecular weight and R_g, using the entire scattering profiles, were estimated using the program GNOM.

Shape prediction analysis

Shape prediction analysis of Miranda CBD was performed using the program GASBOR (Svergun et al. 2001). The protein was represented as an assembly of dummy residues inside a search volume. To define the simulation space used in the calculation, the upper limitation of the maximum linear dimension was set to be 25 nm. Starting from a random structure, a protein-like model was built using a simulated annealing algorithm to fit the experimental scattering profile. Forty independently computed

models were superimposed and averaged using the program package DAMAVER (Volkov and Svergun 2003), resulting in an averaged model structure of Miranda CBD with $D_{max} = 21.7$ nm.

Electronic supplemental material

The result of Dynamic Light Scattering (DLS) measurements are given, which indicate the presence of a monodisperse population of highly elongated molecules of Miranda CBD in solution.

Acknowledgments

We thank Chris Doe for background and providing Miranda cDNA. This work was supported by a research grant from the Japanese society of promotion of science (JSPS) to M.S.Y.

References

Andrade, M.A., Chacón, P., Merelo, J.J., and Morán, F. 1993. Evaluation of secondary structure of proteins from UV circular dichroism using an unsupervised learning neural network. *Protein Eng.* **6:** 383–390.

Betschinger, J. and Knoblich, J.A. 2004. Dare to be different: Asymmetric cell division in *Drosophila*, *C. elegans* and vertebrates. *Curr. Biol.* **14:** R674–R685. doi: 10.1016/j.cub.2004.08.017.

Betschinger, J., Mechtler, K., and Konblish, J.A. 2006. Asymmetric segregation of the tumor suppressor Brat regulates self-renewal in *Drosophila* neural stem cells. *Cell* **124:** 1241–1253.

Brown, J.H., Zhou, Z., Reshetnikova, L., Robinson, H., Yammani, R.D., Tobacman, L.S., and Cohen, C. 2005. Structure of the mid-region of tropomyosin: Bending and binding sites for actin. *Proc. Natl. Acad. Sci.* **102:** 18878–18883.

Chen, Y.H., Yang, J.T., and Martinez, H.M. 1972. Determination of the secondary secondary sturctures of proteins by circular dichroism and optical rotatory dispersion. *Biochemistry* **11:** 4120–4131.

Choksi, S.P., Southall, T.D., Bossing, T., Edoff, K., De Wit, E., Fischer, B.E., Van Steensel, B., Micklem, G., and Brand, A.H. 2006. Prospero acts as a binary switch between self-renewal and differentiation in *Drosophila* neural stem cells. *Dev. Cell* **11:** 775–789.

Cohen, C. and Parry, D.A. 1990. α-Helical coiled coils and bundles: How to design an α-helical protein. *Proteins* **7:** 1–15.

Combet, C., Blanchet, C., Geourjon, C., and Deléage, G. 2000. Network protein sequence analysis. *Trends Biochem. Sci.* **25:** 147–150.

Cooper, T.M. and Woody, R.W. 1990. The effect of conformation on the CD of interacting helices: A theoretical study of tropomyosin. *Biopolymers* **30:** 657–676.

Crick, F.H.C. 1953. The packing of α-helices: Simple coiled coil. *Acta Crystallogr.* **6:** 689–697.

Dong, G., Medkova, M., Novick, P., and Reinisch, K.M. 2007. A catalytic coiled coil: Structural insights into the activation of the Rab GTPase Sec4p by Sec2p. *Mol. Cell* **25:** 455–462.

Eathiraj, S., Mishra, A., Prekeris, R., and Lambright, D.G. 2006. Structural basis for Rab11-mediated recruitment of FIP3 to recycling endosomes. *J. Mol. Biol.* **364:** 121–135.

Fuerstenberg, S., Peng, C.Y., Alvarez-Ortiz, P., Hor, T., and Doe, C.Q. 1998. Identification of Miranda protein domains regulating asymmetric cortical localization, cargo binding, and cortical release. *Mol. Cell. Neurosci.* **12:** 325–339.

Glatter, O. and Kratky, O. 1982. *Small angle X-ray scattering*. Academic Press, London, UK.

Guinier, A. and Fournet, G. 1955. *Small angle X-ray scattering*. Wiley, New York.

Horgan, C.P., Oleksy, A., Zhdanov, A.V., Lall, P.Y., White, I.J., Khan, A.R., Futter, C.E., McCaffrey, J.G., and McCaffrey, M.W. 2007. Rab11-FIP3 is critical for the structural integrity of the endosomal recycling compartment. *Traffic* **8:** 414–430.

Ikeshima-Kataoka, H., Skeath, J.B., Nabeshima, Y., Doe, C.Q., and Matsuzaki, F. 1997. Miranda directs Prospero to a daughter cell during *Drosophila* asymmetric division. *Nature* **390:** 625–629.

King, R.W., Goltzer, M., and Kirschner, M.W. 1996. Mutagenic analysis of the destruction signal of mitotic cyclins and structural characterization of ubiquitinated intermediates. *Mol. Biol. Cell* **7:** 1343–1357.

Kohn, W.D., Kay, C.M., and Hodges, R.S. 1995. Protein destabilization by electrostatic repulsions in the two-stranded α-helical coiled-coil/leucine zipper. *Protein Sci.* **4:** 237–250.

Kohn, W.D., Kay, C.M., and Hodges, R.S. 1997. Salt effects on protein stability: Two-stranded α-helical coiled coils containing inter- or intra-helical ion pairs. *J. Mol. Biol.* **267:** 1039–1052.

Kohn, W.D., Kay, C.M., and Hodges, R.S. 1998. Orientation, positional, additivity, and oligomerization-state effects of interhelical ion pairs in α-helical coiled coils. *J. Mol. Biol.* **238:** 993–1012.

Kulkarni, A. and Rao, M. 2006. Recent developments in proteomics: Mass spectroscopy and protein arrays. *Front. Drug Des. Discov.* **2:** 121–150.

Laemmli, U.K. 1970. Cleavage of structural proteins during the assembly of the head of bacteriophage T4. *Nature* **227:** 680–685.

Lau, S.Y., Taneja, A.K., and Hodges, R.S. 1984. Synthesis of a model protein of defined secondary and quaternary structure. Effect of chain length on the stabilization and formation of two-stranded α-helical coiled coils. *J. Biol. Chem.* **259:** 13253–13261.

Lee, C.Y., Wilkinson, B.D., Siegrist, S.E., Wharton, R.P., and Doe, C.Q. 2006. Brat is a Miranda cargo protein that promotes neuronal differentiation and inhibits neuroblast self-renewal. *Dev. Cell* **10:** 441–449.

Lupas, A., Van Dyke, M., and Stock, J. 1991. Predicting coiled coils from protein sequences. *Science* **252:** 1162–1164.

Mason, J.M. and Arndt, K.M. 2004. Coiled-coil domains: Stability, specificity, and biological implications. *ChemBioChem* **5:** 170–176.

McDonnell, A.V., Jiang, T., Keating, A.E., and Berger, B. 2006. Paircoil2: Improved prediction of coiled coils from sequence. *Bioinformatics* **22:** 356–358.

Monra, O.D., Zhou, N.E., Kay, C.M., and Hodges, R.S. 1993. Comparisons of antiparallel and parallel two stranded α-helical coiled coils. *J. Biol. Chem.* **268:** 19218–19227.

Myers, J.K., Pace, C.N., and Scholtz, J.M. 1997. A direct comparison of helix propensity in proteins and peptides. *Proc. Natl. Acad. Sci.* **94:** 2833–2837.

O'Shea, E.K., Klemm, E.K., Kim, P.S., and Albert, T. 1991. X-ray structure of the GCN4 leucine zipper, a two-stranded, parallel coiled coil. *Science* **254:** 539–544.

Peng, C.Y., Manning, L., Albertson, R., and Doe, C.Q. 2000. The tumour-suppressor genes *lgl* and *dlg* regulate basal protein targeting in *Drosophila* neuroblasts. *Nature* **408:** 596–600.

Richardson, J.M. and Makhatadze, G.I. 2004. Temperature dependence of the thermodynamics of helix–coil transition. *J. Mol. Biol.* **335:** 1029–1037.

Sato, Y., Fukai, S., Ishitani, R., and Nureki, O. 2007a. Crystal structures of the Sec4p.Sec2p complex in the nucleotide exchange intermediate state. *Proc. Natl. Acad. Sci.* **104:** 8305–8310.

Sato, Y., Shirakawa, R., Horiuchi, H., Dohmae, N., Fukai, S., and Nureki, O. 2007b. Asymmetric coiled-coil structure with guanine nucleotide exchange activity. *Structure* **15:** 245–252.

Schuldt, A.J., Adams, J.H.H., Davidson, C.M., Micklem, D.R., Haseloff, J., St. Johnston, D., and Brand, A.H. 1998. Miranda mediates asymmetric protein and RNA localization in the developing nervous system. *Genes & Dev.* **12:** 1847–1857.

Shen, C.P., Jan, L.Y., and Jan, Y.N. 1997. Miranda is required for the asymmetric localization of prospero during mitosis. *Cell* **90:** 449–458.

Shen, C.P., Knoblich, J.A., Chan, Y.M., Jiang, M.M., Jan, L.Y., and Jan, Y.N. 1998. Miranda as a multidomain adapter linking apically localized Inscuteable and basally localized Staufen and Prospero during asymmetric cell division in *Drosophila*. *Genes & Dev.* **12:** 1837–1846.

Shiba, T., Koga, H., Shin, H.W., Kawasaki, M., Kato, R., Nakayama, K., and Wakatsuki, S. 2006. Structural basis for Rab11-dependent membrane recruitment of a family of Rab11-interacting protein 3 (FIP3)/Arfophilin-1. *Proc. Natl. Acad. Sci.* **103:** 15416–15421.

Slack, C., Overton, P.M., Tuxworth, R.I., and Chia, W. 2007. Asymmetric localization of Miranda and its cargo proteins during neuroblast division requires the anaphase-promoting complex/cyclosome. *Development* **134:** 3781–3787.

Svergun, D.I. 1992. Determination of the regularization parameter in indirect-transform methods using perceptual criteria. *J. Appl. Crystallogr.* **25:** 495–503.

Svergun, D.I., Petoukhov, M.V., and Koch, M.H.J. 2001. Determination of domain structure of proteins from X-ray solution scattering. *Biophys. J.* **80:** 2946–2953.

Ueki, T., Hiragi, Y., Kataoka, M., Inoko, Y., Amemiya, Y., Izumi, Y., Tagawa, H., and Muroga, Y. 1985. Aggregation of bovine serum albumin upon cleavage of its disulfide bonds, studied by the time-resolved small-angle X-ray scattering technique with synchrotron radiation. *Biophys. Chem.* **23:** 115–124.

Volkov, V.V. and Svergun, D.I. 2003. Uniqueness of ab initio shape determination in small-angle scattering. *J. Appl. Crystallogr.* **36:** 860–864.

Wodarz, A. 2005. Molecular control of cell polarity and asymmetric cell division in *Drosophila* neuroblasts. *Curr. Opin. Cell Biol.* **17:** 475–481.

Wodarz, A. and Huttner, W.B. 2003. Asymmetric cell division during neurogenesis in *Drosophila* and vertebrates. *Mech. Dev.* **120:** 1297–1309.

Yu, F., Kuo, C.T., and Jan, Y.N. 2006. *Drosophila* neuroblast asymmetric cell division: Recent advances and implications for stem cell biology. *Neuron* **51:** 13–20.

Zhou, N.E., Kay, C.M., and Hodges, R.S. 1992. Synthetic model proteins. Positional effects of interchain hydrophobic interactions on stability of two-stranded α-helical coiled coils. *J. Biol. Chem.* **267:** 2664–2670.

Zhou, N.E., Kay, C.M., and Hodges, R.S. 1994a. The net energetic contribution of interhelical electrostatic attractions to coiled-coil stability. *Protein Eng.* **7:** 1365–1372.

Zhou, N.E., Kay, C.M., and Hodges, R.S. 1994b. The role of interhelical ionic interactions in controlling protein folding and stability. De novo designed synthetic two-stranded α-helical coiled coils. *J. Mol. Biol.* **237:** 500–512.